Bicontinuous Phases in Diblock Copolymer/Homopolymer Blends: Simulation and Self-Consistent Field Theory

Francisco J. Martínez-Veracoechea and Fernando A. Escobedo*

School of Chemical and Biomolecular Engineering, Cornell University, Ithaca, New York 14853

Received October 29, 2008; Revised Manuscript Received December 26, 2008

ABSTRACT: A combination of particle-based simulations and self-consistent field theory (SCFT) is used to study the stabilization of multiple ordered bicontinuous phases in blends of a diblock copolymer (DBC) and a homopolymer. The double-diamond phase (DD) and plumber's nightmare phase (P) were spontaneously formed in the range of homopolymer volume fraction simulated via coarse-grained molecular dynamics. To the best of our knowledge, this is the first time that such phases have been obtained in continuum-space molecular simulations of DBC systems. Though tentative phase boundaries were delineated via free-energy calculations, macrophase separation could not be satisfactorily assessed within the framework of particle-based simulations. Therefore, SCFT was used to explore the DBC/homopolymer phase diagram in more detail, showing that although in many cases two-phase coexistence of a DBC-rich phase and a homopolymer-rich phase does precede the stability of complex bicontinuous phases the DD phase can be stable in a relatively wide region of the phase diagram. Whereas the P phase was always metastable with respect to macrophase separation under the thermodynamic conditions explored with SCFT, it was sometimes nearly stable, suggesting that full stability could be achieved in other unexplored regions of parameter space. Moreover, even the predicted DD- and P-phase metastability regions were located significantly far from the spinodal line, suggesting that these phases could be observed in experiments as "long-lived" metastable phases under those conditions. This conjecture is also consistent with large-system molecular dynamics simulations that showed that the time scale of mesophase formation is much faster than that of macrophase separation.

Introduction

A great deal of attention has been given to diblock copolymer (DBC) systems because of their nanoscale self-assembling properties.[1] These systems can be rationally controlled to form regular mesoscopic morphologies that are exploitable in a vast number of practical applications such as high-porosity materials,[2,3] nanoparticle templating agents, catalytic surfaces, high conductivity nanocomposites,[4] and in dye-sensitized solar cells.[5,6] In fact, it has recently been proposed[7−10] that the most promising morphologies for the achievement of high-efficiency dye-sensitized solar cells are the so-called ordered bicontinuous phases in which the minority (A) component forms two interweaving networks with cubic periodicity, embedded in a continuous matrix of majority (B) component.[11] Among the ordered bicontinuous phases most commonly observed in some amphiphilic systems,[12,13] we have the gyroid (G) phase, the double-diamond (DD) phase, the plumber's nightmare (P) phase, and the Neovius' surface [C(P)] phase. Unfortunately, though, the G phase[14,15] is the only bicontinuous phase that is stable in the pure DBC melt and with a stability region that is relatively narrow compared with other phases such as the lamellar (L) or cylindrical (C) phases.[16,17] Not surprisingly, then, the G phase has received a good deal of attention in both theoretical and simulation studies for a variety of systems such as DBC solutions and melts,[18−21] surfactants,[22,23] tethered objects,[24,25] nanocomposites,[26] and suspensions of pear-shaped particles.[27] However, other bicontinuous phases remain much less studied; the most relevant exception is the triblock copolymer simulations of Dotera.[28]

In the bicontinuous phases, the general structure of the A-component networks can be described in terms of tubes (connectors) and nodes (junction of several tubes).[29] When the A−B interface, to minimize the interfacial energy, tries to approach a constant mean curvature surface, the nodes necessarily become bulkier than the tubes.[29] Therefore, the chains in the nodes find themselves in an entropically unfavorable situation known as packing frustration in which the chains stretch to reach the center of the nodes, a lower concentration region appears in the center of the nodes, the nodes deform, or a combination of all of the above scenarios occurs.[20,21,30] The larger the number of connectors per node, the bulkier the nodes become, causing larger packing frustrations.[29] Whereas the G phase has only three connectors per node, the DD and P phases have four and six connectors per node, respectively, thus explaining the lack of stability of multiple bicontinuous phases in DBC melts. Although in theory the alleviation of packing frustration[30,31] should allow for the stabilization of multiple bicontinuous phases, in practice, it is still unclear how to best accomplish this. Indeed, relevant studies for DBC systems portrayed a rather confusing situation: on one hand, calculations using self consistent field theory (SCFT) predicted the stabilization in a extremely narrow range of the phase diagram, the DD phase by the addition of homopolymer;[32,33] on the other hand, the P phase is the only bicontinuous phase (i.e., other than G) that has actually been found experimentally in inorganic-DBC hybrid systems.[34] In a previous work,[35] we used lattice Monte Carlo (MC) to study the stabilization of multiple bicontinuous phases by blending a G-phase-forming pure DBC system with selective additives that preferentially "like" the A block of the DBC chain. When the additive consisted of small selective-solvent particles, no additional bicontinuous phases were observed; however, when the additive consisted of A-component homopolymer chains, other bicontinuous phases (i.e., the DD and P phases) were observed upon increasing homopolymer concentration. The DD phase was found to be stable in a surprisingly wide range of homopolymer compositions. In addition, we found a novel alternating diameter cylinders (ADC) phase wherein cylinders of two different diameters are arranged in a square packing. A phase similar to the ADC was recently predicted in simulations of a solution of nanoparticles and functionalized block copolymers.[36]

* To whom correspondence should be addressed. E-mail: fe13@cornell.edu.

10.1021/ma802427a CCC: $40.75
Published on Web 02/04/2009

A drawback of particle-based simulations of DBC mesophases is that these phases present long-range periodicity, which makes them prone to finite-size effects; as a consequence, under the same thermodynamic conditions, multiple phases can be spontaneously obtained depending on the simulation box dimensions and (in some cases) the initial conditions.[20,21,28,37,38] Therefore, to establish the stable morphology at each thermodynamic state, a comparison of the molar Helmholtz free energy among the different observed phases (i.e., at a given temperature (T), density (ρ), and composition) must be made.[21] Efficient calculation of accurate pressures in lattice systems is far from trivial; therefore, in discrete space simulations, a common approach has been to approximate Helmholtz free-energy differences by Gibbs free-energy differences under the assumption that the differences in pressure between phases can be neglected.[35] To circumvent this approximation, avoid the inherent problems associated with the discretization of configurational space, and compare with previous results, in this work, we present a continuum-space molecular simulation study of the stabilization of the DD and P phases in a blend of DBC and homopolymer in the intermediate segregation regime. For this purpose, we use MC and molecular dynamics (MD) with a coarse-grained model of the polymer chains in which each bead is represented by the soft-repulsive potential that is typical of the dissipative particle dynamics (DPD) fluid.[39,40] In particle-based molecular simulations, the effects of finite chain length and composition fluctuations are automatically incorporated, and the mesophases are spontaneously formed. Because previous SCFT studies[32] suggest that at the homopolymer concentrations at which the DD and P phases are observed in simulations the stable state could be a two-phase state with a DBC-rich phase and a homopolymer-rich phase, we compare the simulation results with SCFT calculations (which we carried out using the code developed by Morse, Tyler, and coworkers[41]). The SCFT calculations show that although in many cases macrophase separation can indeed precede the stability of complex bicontinuous phases, the DD phase can be stable in a considerably wide region of parameter space. Under the thermodynamic conditions that were explored with SCFT, the P phase was always metastable with respect to macrophase separation. However, in many cases, the P phase was nearly stable, suggesting that there could exist other unexplored regions of the phase diagram where this phase could be fully stable. Moreover, even in the regions where SCFT shows that either the DD phase or the P phase is metastable with respect to macrophase separation, they are found to lie significantly before the spinodal line, suggesting that under those conditions these two phases could be experimentally observed as "very long lived" metastable phases in which the system would probably get "trapped" once formed. Finally, MD simulations of large systems reveal that the time scales needed for mesophase formation are much shorter than those needed for macrophase separation in DBC-rich and homopolymer-rich phases, again suggesting that metastable complex bicontinuous phases could in some cases be experimentally observable.

Simulation Model

We represent polymer chains with a bead-spring model where beads interact with the DPD fluid potential (U^{DPD}) that is widely used in DBC studies[39,40]

$$\frac{U^{DPD}(r)}{kT} = \begin{cases} \dfrac{a_{ij}(1-r)^2}{2} & \text{if} \quad r<1 \\ 0 \quad \text{if} \quad r \geq 1 \end{cases} \tag{1}$$

where r is the interbead distance, a_{ij} is the constant that sets the repulsion strength, and the indices ij can be either the A or the B component. Beads of the same type interact with $a_{ii} = 25$, whereas different-type beads interact with $a_{ij} = a_{ii} + 3.27\chi$, where χ is the Flory−Huggins interaction parameter commonly used in DBC systems. The DBC has a chain length (i.e., number of beads per chain) of $N_{DBC} = 20$, with the first six beads belonging to the A component and the rest to the B component; therefore, the fraction of A-component beads in the DBC chains is $f = 0.30$. The homopolymer length is $N_{ho} = 16$, and all of its beads belong to the A component.

The beads are connected using a harmonic spring potential (U^{har})

$$\frac{U^{har}(r)}{kT} = 1/2k_{sp}r^2 \tag{2}$$

with a spring constant value of $k_{sp} = 4$. Throughout this work, $\chi = 2.25$ (i.e., $\chi N_{DBC} = 45$), and the monomer density was always set to $\rho_o = 3$. It is important to note that the G phase was previously found to be stable under these conditions in the pure DBC melt of this model.[21]

Simulation Methods

Simulations were run in the canonical (nVT) ensemble rather than in the isothermal−isobaric ensemble to avoid the expense of volume moves associated with the latter (for large systems) and for consistency with the constant density SCFT calculations. After generating a random initial configuration at the desired homopolymer volume fraction (ϕ_{ho}), the system was equilibrated using MD. The equations of motion were integrated using the velocity Verlet algorithm[42] with a time step of $\delta t = 0.05$. Temperature was controlled using the time-reversible momentum-preserving Lowe's thermostat[43] in which each pair of particles that lies within a cutoff radius (in this work $r_{cut} = 1$) has its relative velocity randomly thermalized with probability $\Gamma\delta t$ (= 0.05 in this work) at each integration step. We ran simulations for a typical value of 3×10^6 integration steps, although most morphologies were spontaneously formed significantly before (i.e., $<1 \times 10^6$ integration steps) the simulations were finished.

As previously mentioned, at a given thermodynamic state, more than one morphology can be spontaneously formed. Therefore, the stable phase has to be determined by a comparison of the intensive "excess" Helmholtz free energies of each phase and box size. The excess properties are defined by taking as reference an ideal chain with bonded interactions only. The intensive excess Helmholtz free energy can be estimated as

$$\beta a^{ex} = \beta g^{ex} - (Z-1) \tag{3}$$

where $\beta = 1/kT$, $Z = P/\rho_{ch}kT$ is the compressibility factor, ρ_{ch} is the polymer chain number density, and g^{ex} is the intensive excess Gibbs energy

$$\beta g^{ex} = \sum y_i \beta \mu_i^{ex} \tag{4}$$

where y_i is the mole fraction of the i species (i.e., either DBC or homopolymer) and μ_i^{ex} is its excess chemical potential. The compressibility factor (Z) can be accurately calculated directly from an MD simulation using the virial theorem.[42] For this purpose, we used a shorter step of $\delta t = 0.01$, ran simulations that were 2×10^6 steps long, and estimated the uncertainty in the calculated pressure using standard block analysis.[42] To calculate the Gibbs free energy, however, the MC framework becomes more convenient because one can rigorously use the expanded ensemble (EXE) formalism[44,45] and Bennett's acceptance ratio method[46] to calculate the chemical potentials efficiently. Note that either the direct or the configurationally biased test-particle insertion methods fail to provide reliable chemical potential estimates in the dense systems of polymer chains studied here.[21] In the EXE formalism, one gradually inserts/removes a target chain by appending/deleting beads to/

from it. The transitions between macrostates m and $m + \Delta$ of the EXE are accepted/rejected with a weighed Metropolis acceptance rule

$$P_{acc} = \min\{1, \exp(-\upsilon + \psi_{m+\Delta} - \psi_m)\} \quad (5)$$

where $\upsilon = -\Delta \ln W$, $\Delta = +1$ for growth, $\Delta = -1$ for reduction, W is the associated Rosenbluth weight,[42] and the ψ values are arbitrary biasing weights chosen to improve sampling. We use the optimized ensemble method of Trebst et al.[47] to estimate the biasing weights. This method has been used in chemical potential calculations in DBC systems before, and details can be found elsewhere.[21,35,48] Once transitions between macrostates are attempted, the difference in free energy between successive macrostates ($\Delta A_{m,m+1}$) can be efficiently computed using Bennett's acceptance ratio method[46]

$$\beta \Delta A_{m,m+1} \equiv \ln \frac{Q_m}{Q_{m+1}} = C - \ln \frac{l_{m+1,m}}{l_{m,m+1}} \quad (6)$$

where Q_m is the canonical partition function associated with the m^{th} macrostate, $l_{m,m+1}$ is the number of trial transitions from m to $m + 1$, and C is found from

$$\sum\nolimits_m (1 + \exp[\upsilon_{m \to m+1} - C])^{-1} = \sum\nolimits_{m+1} (1 + \exp[\upsilon_{m+1 \to m} + C])^{-1} \quad (7)$$

where the summation in the left runs over all of the $m \to m + 1$ attempted transitions and the summation in the right runs over all of the $m + 1 \to m$ attempted transitions. Finally, the excess chemical potential of a single species can be obtained from

$$\beta \mu_i^{ex} = [\beta A_M - \beta A_1] = \sum\nolimits_{m=1}^{M-1} \beta \Delta A_{m,m+1} \quad (8)$$

where M is the number of macrostates, which in this work is the number of beads in a chain plus one (i.e., $M_{DBC} = 21$ and $M_{ho} = 17$) because we inserted/deleted beads one at a time. Five independent MC simulations (previously equilibrated with MD) were run for each system (with a given mesophase) to improve statistics and to estimate the uncertainty in the chemical potential values. Each of these simulations was run for a total of 10^6 MC cycles, with each cycle comprising four macrostate transition attempts and N_{tot} relaxation moves (i.e., 5% translations, 5% rotations, 20% reptations, 2% switches where a chain is repositioned upside down, 45% hops, and 23% configurational bias moves) with N_{tot} equal to the total number of monomers in the system. To accelerate the decorrelation of the samples further, every 5×10^4 MC steps, the configurations were evolved using MD during 2×10^4 integrations steps of $\delta t = 0.02$ (during which no statistics were collected) and then used as input for the following 5×10^4 MC steps.

Self Consistent Field Theory

In the literature, there are numerous studies where SCFT has been successfully applied to elucidate the phase behavior of DBC systems.[49−51] In addition, homopolymer/DBC blends (though only in the weak segregation regime) have already been studied using SCFT by Matsen.[32] Therefore, here we will only outline the main elements of the theory. (Further details can be found elsewhere.[49−51]) In SCFT, the problem of many interacting DBC and homopolymer chains is replaced by the statistical mechanics of an ideal Gaussian chain in an average position-dependent effective mean-field potential

$$w_A(r) = \chi N \phi_B(r) + \xi(r)$$
$$w_B(r) = \chi N \phi_A(r) + \xi(r) \quad (9)$$

where $N = N_{DBC}$ and the field $\xi(r)$ is a Lagrange multiplier that allows us to enforce the incompressibility constraint

$$\phi_A(r) + \phi_B(r) = 1 \quad (10)$$

Once the w fields have been specified, the whole statistical mechanics of the system can be expressed in terms of the chain propagators [$q_{DBC}(r,s)$ and $q_{ho}(r,s)$] for the DBC and the homopolymer, respectively, that satisfy the following differential equation

$$\frac{\partial q_{DBC}(r,s)}{\partial s} = \frac{b_i^2 N}{6} \nabla^2 q_{DBC}(r,s) - w_i(r) q_{DBC}(r,s) \quad (11)$$

with the initial condition $q_{DBC}(r,0) = 1$. Here s is a contour variable ($0 \le s \le 1$) and i satisfies

$$i = \begin{cases} A & \text{if } s < f \\ B & \text{if } s > f \end{cases} \quad (12)$$

and b_i is the statistical segment length of the i component. The homopolymer chain propagator $q_{ho}(r,s)$ satisfies an equation similar to eq 11 but with $i = A$ and $s \in [0,\alpha]$ with $\alpha = N_{ho}/N_{DBC} = 0.8$.

The local volume fraction of the A component is obtained by

$$\phi_A(r) = \frac{(1-\phi)}{Q_{DBC}} \int_0^f ds\, q_{DBC}(r,s) q^c_{DBC}(r,s) + \frac{\phi}{\alpha Q_{ho}} \int_0^\alpha ds\, q_{ho}(r,s) q_{ho}(r, \alpha - s) \quad (13)$$

whereas ϕ_B is found from

$$\phi_B(r) = \frac{(1-\phi)}{Q_{DBC}} \int_f^1 ds\, q_{DBC}(r,s) q^c_{DBC}(r,s) \quad (14)$$

with the complementary propagator, q^c_{DBC}, obtained from an equation similar to eq 11 but with the right-hand side multiplied by -1 and with the initial condition $q^c_{DBC}(r,1) = 1$. The single DBC-chain partition function Q_{DBC} is defined as

$$Q_{DBC} \equiv \frac{1}{V} \int_V dr\, q_{DBC}(r,1) \quad (15)$$

with a similar expression for Q_{ho} but with $q_{DBC}(r,1)$ replaced by $q_{ho}(r,\alpha)$. Finally, the Helmholtz free energy can be estimated as

$$\frac{FN}{nkT} = (1-\phi)\left[\ln\left(\frac{1-\phi}{Q_{DBC}}\right) - 1\right] + \frac{\phi}{\alpha}\left[\ln\left(\frac{\phi}{Q_{ho}}\right) - 1\right] + \frac{1}{V} \int dr \left[\phi_A \phi_B \chi N - \sum_{i=A,B} w_i \phi_i\right] \quad (16)$$

Equations 9 through 15 form a closed set of equations that can be numerically solved self-consistently and have the w fields as independent variables. In this work, these equations were solved using the code developed by Morse, Tyler, and coworkers[41] in which the w fields were efficiently obtained by expanding them in symmetry-adapted basis functions that could be automatically generated for any space group,[52] eq 11 was solved using a fourth-order operator splitting integration algorithm,[53] and finally, an efficient mechanical-stress calculation provided a convenient algorithm for simultaneously iterating on the unit cell size and the w fields.[54] Because this approach requires the symmetry of the desired morphologies to be specified before solving the mean-field equations, it is important to note that the G, DD, and P phases belong to the space groups $Ia\bar{3}d$, $Pn\bar{3}m$, and $Im\bar{3}m$, respectively.

Results and Discussion

Molecular Simulation. Simulations were carried out at $\chi N = 45$ in a range of homopolymer volume fraction of $0.13 \le \phi_{ho} \le 0.30$. Under these conditions, four distinct morphologies were spontaneously formed: the phases P, DD, and C and in a

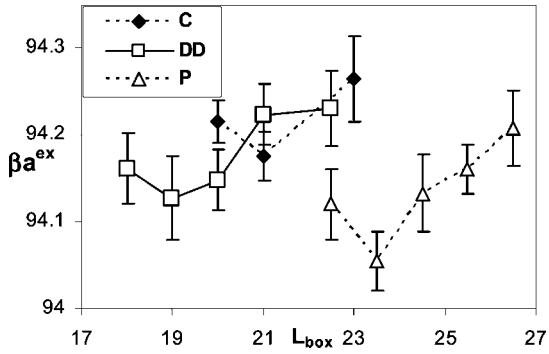

Figure 1. Plot of βa^{ex} as a function of the simulation box size, L_{box}, for the C, DD, and P phases at $\phi_{ho} = 0.30$. For each phase, βa^{ex} is seen to reach a minimum value, which is then used to determine the stable phase.

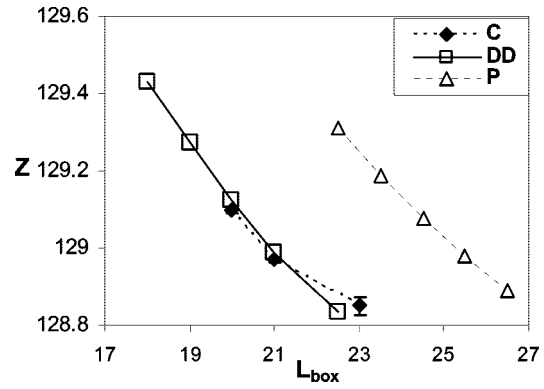

Figure 2. Compressibility factor (Z) as a function of L_{box} for different competing phases at $\phi_{ho} = 0.30$.

few cases, the perforated lamellar (PL) phase. To the best of our knowledge, this work constitutes the first report that the DD and P phases have been obtained in continuum-space particle-based simulations of DBC systems. The PL phase only formed in very small simulation boxes where none of the other phases could fit a complete unit cell; for this reason, we safely disregard the PL as a finite-size artifact. To establish which phase is the stable phase among the other three phases, at each value of ϕ_{ho}, we calculated βa^{ex}, as explained in the Simulation Methods. Because of the long-range periodicity of the morphologies, the calculated values of the free energy were a function of the simulation box size (L_{box}), which demonstrates that the wrong choice of simulation box size can cause an extra free-energy penalty on a given phase and therefore induce the formation of a metastable phase instead of the "true" stable one. As an example, in Figure 1, we present a plot of βa^{ex} against L_{box} for the C, DD, and P phases at $\phi_{ho} = 0.30$. For each phase, βa^{ex} is seen to reach a minimum value, which is then used to determine the stable phase. Under these conditions, the P phase was found to be stable because it has the lowest value of βa^{ex}. In some cases, to obtain a given phase at several values of L_{box}, we took a spontaneously formed morphology at the desired value of ϕ_{ho}, compressed/expanded it slightly, removed/added polymer chains to keep ρ_o and ϕ_{ho} constant, and then equilibrated it using MD. However, when the phases were at L_{box} values that were far enough from the equilibrium value (i.e., minimum free energy), they often spontaneously evolved to another phase, thus limiting the number of available points for each phase in Figure 1. As expected, for a given phase, the value of Z (proportional to the pressure) increases with decreasing L_{box} (Figure 2). However, the location of the minimum in the excess Helmholtz energy is a compromise between the behavior of Z and the complex dependence of the excess chemical potentials of the

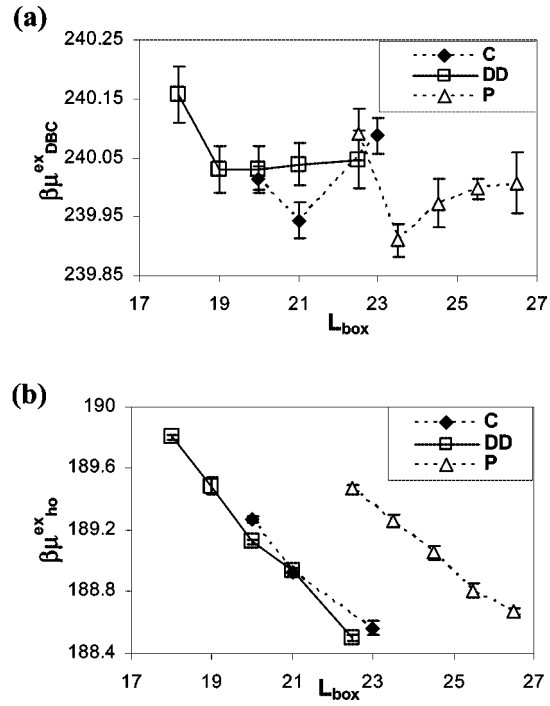

Figure 3. Excess chemical potentials, $\beta\mu^{ex}$, for the C, DD, and P phases at $\phi_{ho} = 0.30$. (a) DBC excess chemical potential and (b) homopolymer excess chemical potential.

two species. At $\phi_{ho} = 0.30$ for example, whereas the DBC $\beta\mu^{ex}$ (Figure 3a) follows a nontrivial behavior with box size (often showing a minimum), the homopolymer $\beta\mu^{ex}$ (Figure 3b) clearly increases with decreasing L_{box}, which is consistent with the idea that a smaller L_{box} implies a stronger confinement of the homopolymer inside smaller A-domain regions, reducing its configurational entropy and hence increasing its chemical potential. (A similar behavior is observed for all values of ϕ_{ho}.)

One shortcoming of the free-energy analysis presented above is that the simulations were performed in relatively small systems, with only one unit cell for the DD and P phases and with just a few unit cells for the C phase; therefore, finite-size effects can be important. (In Figures 1−3, the total number of "mers" per box can be found from no. mers $= \rho_0 L_{box}^3$). In an attempt to assess these effects in each phase while keeping the systems computationally tractable, we took the already equilibrated systems at the sizes at which the free energy is a minimum and doubled them in size (i.e., doubling only one dimension); we then equilibrated them using MD and calculated their free energy in the same way as that for the "smaller" systems but with MC simulations that were run by a total of 2×10^6 cycles. Whereas the initial morphology was usually preserved, in some cases, it either developed some defects or was destroyed. When this happened, we took the equilibrated systems with sizes that were "neighboring" the free-energy minimum, doubled them, and calculated the free energy. Interestingly, smaller sized systems (i.e., to the left of the minimum) tended to get destroyed more often when doubled in size than larger systems (i.e., to the right of the minimum), which suggests that some of these small-box structures were being artificially stabilized by finite-size effects.

After performing a similar free-energy analysis for the simulations obtained at different values of ϕ_{ho}, we obtained the approximate phase diagram shown in Figure 4a, where we have delineated tentative phase boundaries to indicate the regions of stability of each phase. In Figure 4b, we plot the difference in excess Helmholtz free energy between the different morphologies and the C phase at the different values of ϕ_{ho} (i.e., $\Delta\beta a^{ex}$

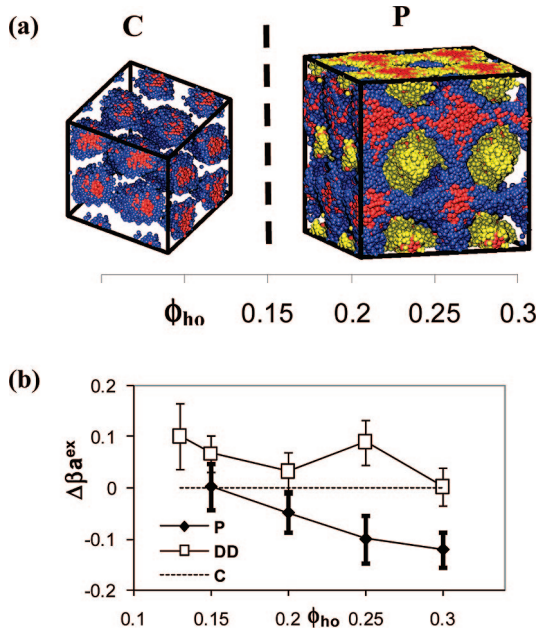

Figure 4. (a) Approximate phase diagram obtained with the particle-based simulations as a function of ϕ_{ho} for $\chi N = 45$. The regions of stability of each phase are roughly delineated on the basis of free-energy calculations. Snapshots of the C and P phases are shown, whereas the B component has been omitted for clarity. In the C phase, the A blocks are shown in blue. In the P phase, the A blocks are shown in either blue or yellow depending on which minority-component network they belong to. The homopolymer is shown in red. (b) Helmholtz free-energy difference ($\Delta\beta a^{ex}$) of the distinct phases with respect to the C phase. The DD phase was never found to have the lowest free energy at the discrete values of ϕ_{ho} studied. The C−P phase transition is located around $\phi_{ho} \approx 0.15$.

$\equiv \beta a^{ex}{}_i - \beta a^{ex}{}_C$, with i = P, DD, or C). The free energies employed in this plot were estimated from the double-size systems previously mentioned. For clarity, we show the (dashed) curve $\Delta\beta a^{ex} = 0$, indicating the excess free energy of the C phase. Interestingly, the DD phase never has the lowest free energy despite spontaneously forming in the simulations, whereas the P phase is the stable phase over most of the composition range studied. However, at $\phi_{ho} = 0.15$, the free energy of the P phase is (within error bars) essentially equal to the free energy of the C phase. Because packing frustration will destabilize the P phase at lower homopolymer volume fractions and the P phase was not spontaneously formed in the simulations at $\phi_{ho} = 0.13$, we conclude that the C−P phase boundary is located around $\phi_{ho} \approx 0.15$. Finally, we expect the existence of a G−C phase transition at even lower values of ϕ_{ho} (i.e., outside the composition range studied) because the G phase has been shown to be stable in the pure melt of this model system (i.e., $\phi_{ho} = 0$).[21] In summary, the simulation model is consistent with the sequence G → C → P as ϕ_{ho} increases.

Comparison with Self-Consistent Field Theory. Molecular simulations present the advantage of the morphologies forming spontaneously when started from random configurations, and thus little previous information about the symmetry of the morphologies is often needed. However, accurate calculation of the free energy of each phase is computationally demanding and no automatic and robust method for determining the appropriate unit cell dimensions of each phase is available to date. Moreover, molecular simulation cannot satisfactorily assess macrophase separation in DBC systems because of the large simulation sizes and long time scales involved. For this reason, once a set of plausible morphologies has been obtained from simulation, it proves convenient to use SCFT for exploring the phase diagram of the DBC/homopolymer blend in a faster, broader, and more detailed fashion.

We explored the phase diagram using SCFT in a range of homopolymer composition of $0 \le \phi_{ho} \le 0.40$ and segregation of $25 \le \chi N \le 35$. In this range of segregation (i.e., intermediate segregation regime), the observed morphologies are less likely to be destroyed by fluctuation effects, as has been shown to occur in the weakly segregated region of the phase diagram.[55,56] Note that whereas the simulations were performed at a higher value of segregation (i.e., $\chi N = 45$), such a high value of χN becomes computationally prohibitive for the solution of the SCFT equations given the large number of basis functions needed for an accurate enough description. However, we expect that the phase behavior predicted by SCFT at $\chi N = 45$ should be similar to that observed at $\chi N \approx 35$. This expectation is supported by the weak dependence of the phase boundaries' location on χN once a high-enough segregation has been reached (i.e., $\chi N \ge 30$). (See discussion below.)

Exact correspondence between simulation results and SCFT is not possible. In the simulations, only certain values of f are accessible because of the discretization caused by the finite number of beads (e.g., $N_{DBC} = 20$). In addition, finite chain-length effects, fluctuations, and differences in the underlying model will cause differences in the observed phase diagrams. However, it is expected that the general features of the phase diagram (e.g., sequence of stable phases, etc.) will remain qualitatively the same. Whereas in the particle-based simulations, the G phase is stable at $f = 0.30$ for the pure system,[21] this is not the case for the Gaussian chains used in SCFT.[17] For this reason, we calculated phase diagrams using SCFT for several values of f, which roughly comprise the region of parameter space for which the G phase is found to be stable in the pure system for $25 \le \chi N \le 35$. The different values studied were $f = (0.315, 0.320, 0.325, 0.330)$, with the first two being close to the transition between the C and G phases in the pure system, a region of the phase diagram that is analogous to where the computer simulations were carried out.

In Figure 5a, we show the predicted phase diagram in a χN versus ϕ_{ho} plot for $f = 0.315$. The C phase is the only morphology found to be stable under these conditions. The system macrophase separates in the DBC-rich C phase and in a homogeneous homopolymer-rich (HoR) phase, although the G phase is expected to be stable in the pure system for $\chi N > 41$. The HoR phase was found to be essentially pure homopolymer (i.e., $\phi_{ho} > 0.99999$) in the range of parameters studied (including the different values of f). In Figure 5b, we present the regions of the phase diagram where distinct phases have the lowest Helmholtz free energy, that is, what the phase diagram would be if macrophase separation were disallowed. This type of plot allows a comparison with molecular simulation results where the relatively small simulations boxes used would preclude macrophase separation. Figure 5b shows that the addition of homopolymer reduces the free energy of the DD and P phases with respect to the other phases. However, for $f = 0.315$, the region of "metastability" of the DD phase is very narrow. In fact, for low χN (i.e., < 28.87), the DD no longer has a region of lowest free energy. Figure 5b also shows, in dashed line, the boundary where macrophase separation occurs. It is interesting that even though the phases to the "right" of the dashed-line are metastable with respect to macrophase separation, they are outside of their own spinodal curve (not shown), which is given by the condition

$$\frac{\partial^2 F}{\partial \phi_{ho}^2} = 0 \qquad (17)$$

which suggests that the system could remain trapped in one of these metastable phases as a single-phase long-lived metastable

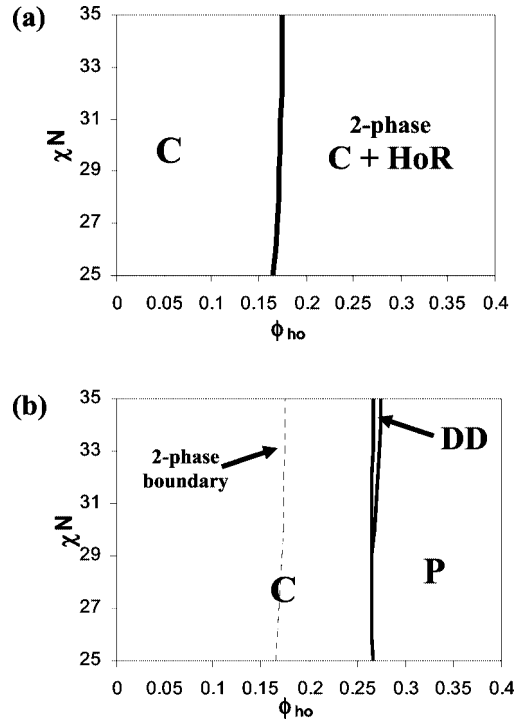

Figure 5. Plot of the SCFT predictions in a χN versus ϕ_{ho} diagram for $f = 0.315$. (a) Stable phase diagram. The C phase is the only stable morphology under the conditions studied. At a great enough homopolymer concentration, the system presents macrophase equilibrium between the C phase and an almost-pure homopolymer-rich (HoR) phase. (b) Regions of phase diagram where the different competing phases have the lowest free energy. The macrophase separation coexistence line is shown (dashed). The DD and P phases are metastable with respect to macrophase separation. The region of metastability of the DD phase is quite narrow.

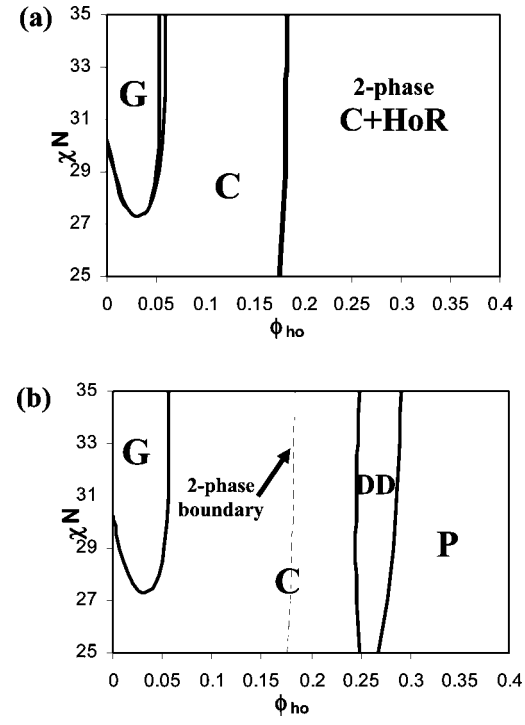

Figure 6. χN versus ϕ_{ho} diagram calculated with SCFT for $f = 0.32$. (a) Stable phase diagram. The G phase is initially stabilized by small amounts of homopolymer, but further addition produces a transition toward the C phase. At high homopolymer concentration, the system presents a macrophase equilibrium between the C phase and the HoR phase. (b) Regions of phase diagram where the different competing phases have the lowest free energy. The macrophase separation coexistence line (dashed) indicates that the DD and P phases are metastable with respect to macrophase separation. The region of metastability of the DD phase increases with respect to the $f = 0.315$ case.

state before macrophase separating. The ADC phase was found to always have higher free energy than the other phases. (This was also true for all of the values of f studied.)

Figure 6a shows the calculated phase diagram in a χN versus ϕ_{ho} plot for $f = 0.32$. The region of stability of the G and C phases is separated by a narrow region where they both coexist. At $\chi N > 30.2$, the G phase is stable in the pure system and remains stable for low homopolymer concentrations. Further addition of homopolymer eventually destabilizes the G phase, and the C phase becomes stable. For $\chi N < 30.2$, the C phase is stable in the pure system; however, a transition of the form C $\rightarrow$ G $\rightarrow$ C is observed for a finite range of χN that culminates in an azeotrope around $\chi N \approx 27.3$ and $\phi_{ho} \approx 0.03$. This is remarkable because it shows that the addition of small amounts of homopolymer (i.e., $\phi_{ho} \approx 0.03$) can stabilize the G phase in areas of the phase diagram where the C phase is the stable phase in the pure system. This is consistent with the idea that the reason for the limited stability of the bicontinuous phases in the DBC melt is packing frustration inside the nodes and that the addition of small amounts of homopolymer can relieve this frustration in the G phase. For higher values of ϕ_{ho}, nonetheless, the C phase becomes stable until the point where macrophase separation occurs, wherein the C phase coexists with a HoR phase. Similarly, Figure 6b shows the phase diagram regions where the distinct phases have the lowest Helmholtz free energy and (in dashed line) the boundary where macrophase separation occurs. To the right of the dashed line, we observe the DD and P phases, with the DD phase occupying a larger region of phase diagram than with $f = 0.315$. Although the DD and P phases are metastable with respect to macrophase separation, they could be "long-lived" because their regions of lowest free energy (as a single phase) are outside of their spinodal curves. Figure 6b shows how in a system where macrophase separation is prevented (e.g., in simulation of small systems) one could observe a progression of phases with the addition of homopolymer like G $\rightarrow$ C $\rightarrow$ DD $\rightarrow$ P. In a previous work,[35] we performed lattice simulations of DBC/homopolymer blends where we observed precisely such a progression. Although in that work we found that there was a significant region in which the C phase had lower free energy than the G and DD phases, we erroneously assumed that the C phase was just metastable (because of the lack of any precedence for a G-to-C transition induced by the addition of selective additive). However, the SCFT calculations together with the previous free-energy calculations amount to enough evidence to conclude that the C phase is the true stable phase in the region of phase diagram between the G and DD phases.

In Figure 7a, we show the calculated phase diagram in a χN versus ϕ_{ho} plot for $f = 0.325$. The observed phase behavior is qualitatively similar to that of the $f = 0.32$ case but with an enlarged region of stability for the G phase because the G phase is now stable in the pure system for $\chi N > 25.5$. The addition of enough homopolymer (i.e., $\phi_{ho} \approx 0.08$) destabilizes the G phase in favor of the C phase. In Figure 7b, we show the regions where each phase has the lowest free energy together with the macrophase separation coexistence line (dashed). The free energies of the DD and P phases are seen to be lowered by the addition of homopolymer because of reduction in the packing frustration but not enough to become stable phases. The region where the DD phase is metastable is considerably larger now than for smaller values of f, and the region where the DD phase has the lowest free energy is closer to the two-phase coexistence curve.

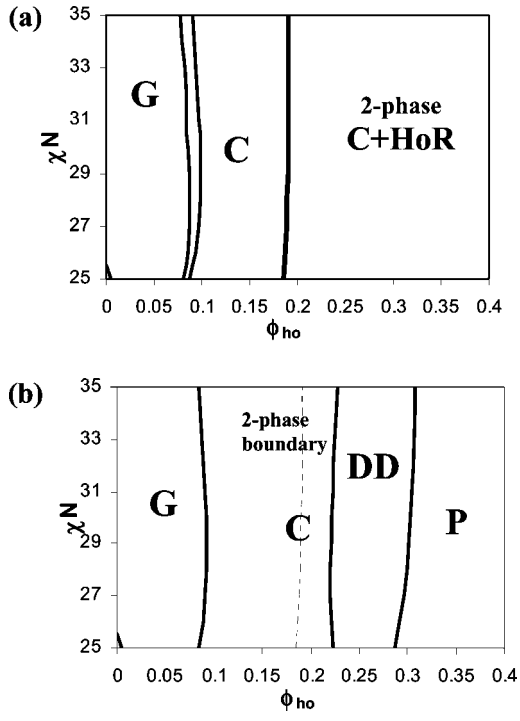

Figure 7. SCFT diagram of χN versus ϕ_{ho} for $f = 0.325$. (a) Phase diagram. The G phase is stable in a significant region of the phase diagram for low homopolymer content, but the C phase becomes stable for moderate homopolymer content. A further increase in ϕ_{ho} eventually leads to the coexistence of the C phase and the HoR phase. (b) Regions of phase diagram where the different competing phases have the lowest free energy. The macrophase separation coexistence line is also shown (dashed). The DD and P phases are metastable with respect to macrophase separation; however, the region of metastability of the DD phase is near the coexistence line.

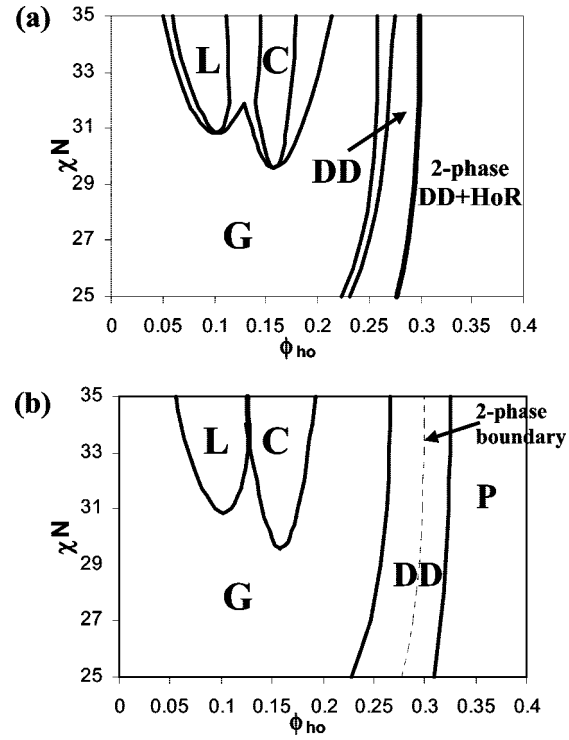

Figure 8. χN versus ϕ_{ho} diagram of the SCFT calculations for $f = 0.33$. (a) Phase diagram. The DD phase is stable in a significant region of the phase diagram. A triple point where the L, G, and C phases coexist is observed. A complex progression of phases with the addition of homopolymer can be observed, including the remarkable sequence G → L → G → C → G → DD for $\chi N \approx 31.5$. A further increase in ϕ_{ho} eventually causes the coexistence of the DD phase and the HoR phase. (b) Regions of phase diagram where the different competing phases have the lowest free energy. The macrophase separation coexistence line is also shown (dashed). The P phase is still metastable with respect to macrophase separation.

Figure 8a presents the calculated phase diagram for $f = 0.33$. The observed phase behavior is significantly complex, with the more distinguishing feature being that the DD phase is now the most stable state in a significant region of phase diagram that should be wide enough, in both χN and ϕ_{ho}, to be experimentally attainable. Therefore, this work constitutes an extension of the previous work of Matsen,[32] where the DD phase was found to be stable in only a very narrow region of the phase diagram. It is important to note that to date, the DD phase has never been experimentally observed in melts of DBC systems;[14,57,58] we hope that the present results will contribute to changing this situation.

Figure 8a also shows how the L phase starts to be stabilized with increasing χN, reflecting the fact that we are approaching the f and χN values where the G−L phase boundary occurs in the pure system.[59] In the same way, the C phase region becomes much smaller, which is consistent with the fact that the C phase is losing stability because of the increasingly longer minority-component block. In between the single-phase regions there are, as expected, regions of coexistence; in particular, there is a triple point around $\chi N = 31.885$, where the L, G, and C phases coexist and have homopolymer volume fractions (ϕ_{ho}) of 0.114, 0.130, and 0.140, respectively. In addition, the coexistence regions between the L and G phases and between the G and C phases end in azeotropes when lowering χN. The very wide range of ϕ_{ho} for which the G phase is stable at low χN is a consequence of the fact that under these conditions the G phase is at the very core of its region of stability in the pure system. For values of χN between the L−G azeotrope (i.e., $\chi N \approx 30.85$) and the triple point (i.e., $\chi N \approx 31.885$), the remarkable sequence of stable phases G → L → G → C → G → DD can be observed upon increasing homopolymer content, which gives an idea of the complex interplay of the different factors (i.e., energetic and entropic) that determine the free energy of each one of the competing phases in the system. However, it is likely that thermal fluctuations that become important in the proximity of critical points will have an important effect on the actual sequence of phases that can be experimentally observed.[60] Finally, if the homopolymer content of the DD phase is further increased, then the system macrophase separates into a DBC-rich DD phase and an HoR phase. In Figure 8b, we show the regions where each phase has the lowest free energy together with the macrophase separation coexistence line (dashed). It can be observed that close to the region where the system reaches the maximum of homopolymer solubility (i.e., coexistence line), the P phase exists as a metastable state (again outside the spinodal curve). Given the proximity of these regions, it seems quite feasible to reach a high enough degree of "oversaturation" in homopolymer content to make the P phase experimentally observable. Moreover, this very proximity of the P phase to the stable region strongly suggests that there could be different combinations of χN, f, and α where the P phase becomes fully stable in DBC/homopolymer blends. Finding such a region, however, will be the subject of future work. Also, near the high homopolymer concentration region where the P phase is metastable, other complex bicontinuous phases (e.g., C(P), I-WP, etc.)[12] could have a region of metastability; these phases, however, would have unit cells much larger than our current computational capabilities allow and therefore are outside the scope of the present work.

In the present study we have lowered the free energy of the DD and P phases by the addition of minority-component

homopolymer that is 2.67 times longer than the minority block (c.f., $\alpha = 0.80$ and $f = 0.30$). Under these conditions, the homopolymer is not expected to penetrate into the A-block-rich region (dry brush regime[1]) and hence induces either the formation of phases of more interfacial curvature such as the DD and P phases[35] or macrophase separation. Conversely, when the size of the homopolymer is comparable to or smaller than the affine block (in this case, the A block), the homopolymer swells the affine block (wet brush regime[1]), which induces phases of less interfacial curvature (e.g., L, reverse G, reverse C, etc.) and therefore precludes the formation of the P and DD phases.[35,61] This is consistent with the experimental work of Mareau et al.,[62] where the addition of homopolymer of a size corresponding to the wet brush regime induced the formation of the (reverse) G and C phases but not the DD or P phases under conditions wherein the pure DBC melt formed the L phase.

The fact that two totally different approaches, namely, continuum space particle-based simulations and SCFT, predict the DD and P phases that have a lower free energy than any other single phase at high homopolymer content suggests that this kind of behavior is very general and should apply to many different real DBC/homopolymer systems. This idea is reinforced when considering that these phases were also observed using lattice MC techniques.[35]

Our simulations using the DPD fluid found that for the discrete values of ϕ_{ho} studied the DD phase always had higher free energy than the C and P phases. This is qualitatively what would be observed in SCFT calculations if the "effective" value of the simulation f were in the range of $0.315 < f < 0.320$ because under these conditions, the G phase starts to be stable in the pure system for high χN and the DD phase has the lowest free energy in a very narrow region that could have easily been "skipped" by our choice of discrete ϕ_{ho} values. Interestingly, the previous lattice simulations[35] do present a region where the DD phase has the lowest free energy, suggesting that for the lattice system, the effective value of f is somewhat higher (i.e., $0.32 < f < 0.325$). However, it is important to remember that quantitative comparison between the different approaches is not possible, not only because of the very different nature of the underlying models but also because of the different values of χN employed in each one of the approaches. Because of these reasons, refining the simulation grid to investigate whether the phase diagrams obtained from the different approaches further agree could prove to be unproductive.

Although we cannot directly measure the concentration at which the system phase-separates in the DPD-fluid simulations, SCFT calculations for $f < 0.325$ suggest that the regions where our simulations find the DD and P phases with the lowest free energy are metastable with respect to macrophase separation in DBC-rich and HoR phases. However, the same SCFT calculations also show that at these high values of χN these phases are not unstable and could therefore be long-lived metastable states. Therefore, whether the DD and P phases can be experimentally observed for $f < 0.325$ is going to depend on the kinetics of mesophase formation and macrophase separation. Although making such a kinetic study lies outside of the scope of the present work, we used MD simulations to get an order-of-magnitude estimate of the difference between the time scales needed for mesophase formation and for macrophase separation. Because macrophase separation can be inhibited because of the free-energy penalty incurred to create an interface in a relatively small simulation box,[42] we set one dimension to be much longer than the other two to induce the formation of the interface perpendicular to the long direction and allow for two well-defined bulk phases.[63] Accordingly, the simulation box had dimensions of $22 \times 22 \times 150$ DPD units, and the initial configuration was a random mixture of the DBC and homopolymer at the desired volume fraction (i.e., $\phi_{ho} = 0.30$), which is expected to be in the metastable region of phase diagram. The system was then evolved using MD for a long simulation time (i.e., 1×10^7 steps of $\delta t = 0.05$). Although a mesophase was readily observed, no signs of macrophase separation were ever found. For this reason, we decided to induce the macrophase separation by "seeding" a homopolymer-rich nucleus. To create such an initial configuration, a significant portion (i.e., 20%) of the box was filled with pure homopolymer, whereas the remainder of the box was filled with a DBC/homopolymer blend of the desired homopolymer volume fraction (i.e., $\phi_{ho} = 0.30$). The system was evolved again using MD for a long simulation time (i.e., 2×10^7 steps of $\delta t = 0.05$). Interestingly, whereas the DBC/homopolymer section of the simulation box rapidly (i.e., before 5×10^5 steps) segregated into A-rich and B-rich domains, no significant diffusion of homopolymer between the two phases was observed. Moreover, the DBC/homopolymer blend initially arranged into two different sections in which the DD phase and the ADC phase were identified ($<2 \times 10^6$ steps) (Figure 9a). Afterward, the DD phase section started to grow at the expense of the ADC phase until after $\sim 3.5 \times 10^6$ simulation steps, when the DBC/homopolymer blend was entirely arranged in the DD phase (Figure 9b). Nonetheless, during the whole simulation run (i.e., 2×10^7 steps), no homopolymer was able to go from the DBC/homopolymer section to the homopolymer rich phase, indicating that the kinetics of phase separation is at least (but probably more than) one order of magnitude slower than that of mesophase formation. To understand this difference in time

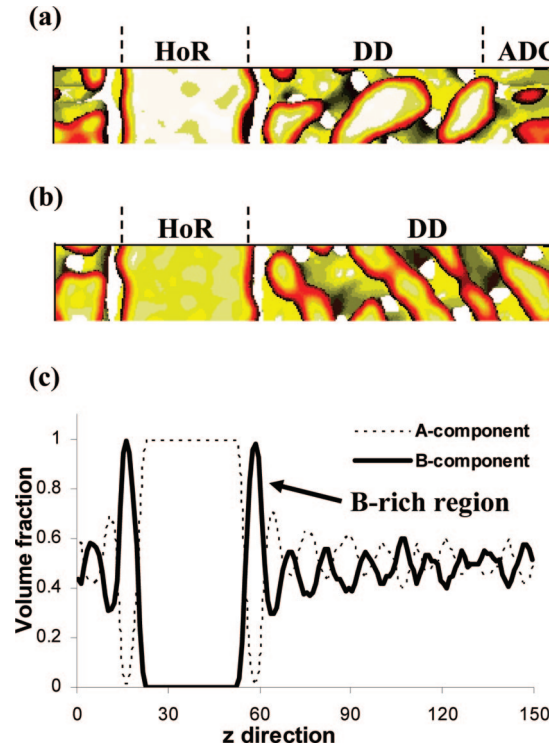

Figure 9. MD simulation in a box with dimensions of $22 \times 22 \times 150$ DPD units. The initial configuration was seeded with a homopolymer-rich nucleus, whereas the remainder of the box was filled with a DBC/homopolymer blend of $\phi_{ho} = 0.30$. (a) Snapshot after 2×10^6 integration steps. Two different regions, one with the DD phase and one with the ADC phase, can be observed. Only the A component is shown. (b) Snapshot after 3.5×10^6 integration steps where the DD phase has taken over the whole system. (c) Concentration profile of the previous snapshot; close to the interface, there is a region of almost pure B component that prevents the diffusion of the homopolymer chains across the interface.

scales, the structure of the interface is examined in the concentration profile shown in Figure 9c, where it can be seen that even after a homopolymer-rich nucleus has been formed, the homopolymer molecules would need to diffuse across a nearly pure B-component region to reach the HoR phase and therefore incur a very high energetic penalty. Therefore, the interface literally acts as an impermeable barrier that frustrates the macrophase separation process by preventing direct diffusion of the homopolymer chains. The origin of the B-rich domain close to the interface is easily understood when considering that the DBC chains in the vicinity of the HoR nucleus have to position their A-blocks so that they are in contact with the HoR phase, thus effectively "coating" the whole homopolymer-rich nucleus with DBC B blocks. This being the case, macrophase separation needs to rely on other mechanisms to transport the homopolymer chains such as interfacial defect formation and large density fluctuations. However, it is likely that given the highly dense systems studied here such events are too rare to be directly observed in simulations (in the absence of external forces such as shearing action). Nevertheless, mesophase formation involves only local rearrangement of DBC and homopolymer chains, a process that is significantly faster. It is possible that for real systems where the interfacial area is much larger than that of the simulated systems, interfacial defects may occur that would accelerate the process of macrophase separation. However, in our simulations, we never observed the formation of such defects, not even when the cross section of the simulation box was made to be as large as 40×40 DPD units. This result suggests that even if the stable state is macrophase separation and if a sample is prepared from a homogeneous, quiescent state where the DBC and homopolymer chains are well mixed, the system will tend to form a mesophase prior to macrophase separation and could perhaps remain trapped in this state for time scales long enough for experimental measurement.

Conclusions

We have shown how a combination of particle-based simulations and SCFT can be used to gain a better understanding of the complex phase behavior of DBC/homopolymer blends. In the continuum-space particle-based simulations, the ordered bicontinuous DD and P phases were spontaneously formed without previous information about their symmetry. To the best of our knowledge, this is the first time that these two phases have been obtained in continuum-space molecular simulations of DBC systems. Additionally, the simulated phases in the present work are consistent with those of a previous simulation work of DBCs in discrete space.[35] However, particle-based simulations possess the disadvantage that free-energy calculations are expensive and that phase separation is difficult to deal with. Conversely, calculations of free energy and phase equilibrium are straightforward in SCFT, but this requires information about the symmetries of the candidate phases. Therefore, once simulations provided an idea of the possible phase behavior, we proceeded to use SCFT to analyze the DBC/homopolymer phase diagram in more detail. The SCFT calculations showed that although in many cases macrophase separation can indeed precede the stability of complex bicontinuous phases, the DD phase can be stable in a considerably wide region of the phase diagram around $f \approx 0.33$ and $\phi_{ho} \approx 0.26$. We hope that the present work will prompt experimental efforts to try to confirm the formation of the DD phase in DBC systems. SCFT also showed how a small amount of homopolymer can stabilize the G phase in regions of the phase diagram where it is not stable in the pure system, whereas a further increase in ϕ_{ho} can actually stabilize the C phase. Under the thermodynamic conditions that were explored with SCFT, the P phase was always metastable with respect to macrophase separation. However, the proximity of the P-phase metastability region to the two-phase (i.e., DBC-rich and HoR) coexistence line suggests that there could be other regions of parameter space where the P phase is fully stable. Moreover, even when the DD and P phases are only metastable, MD simulations suggests that the kinetics of mesophase formation is at least one order of magnitude faster than the kinetics of macrophase separation, which indicates that these phases might be able to be experimentally observed as "long-lived" metastable states.

Finally, we showed that the problem of stabilizing multiple bicontinuous phases was equivalent to the problem of overcoming packing frustration while avoiding macrophase separation. In the present work, we attempted to perform this stabilization using a linear homopolymer with a chain length of $\alpha = 0.8 \times N_{DBC}$. Although this size and architecture of the selective additive accomplished many of the desired objectives, it is not necessarily optimal. In a future work we will study the effects that alternative features of the selective additive have on the stabilization of multiple ordered bicontinuous phases.

Acknowledgment. We thank Prof. David Morse and his student Jian Qin for providing the code and generous guidance to implement the SCFT calculations. We also thank Prof. U. Wiesner for helpful discussions. The financial support by the NSF (grant 0756248) and by the Cornell-KAUST center is gratefully acknowledged.

References and Notes

(1) Hamley, I. W. *The Physics of Block Copolymers*; Oxford University Press: New York, 1998.
(2) Uehara, H.; Yoshida, T.; Kakiage, M.; Yamanobe, T.; Komoto, T.; Nomura, K.; Nakajima, K.; Matsuda, M. *Macromolecules* **2006**, *39*, 3971–3974.
(3) Kamperman, M.; Garcia, C. B. W.; Du, P.; Ow, H. S.; Wiesner, U. *J. Am. Chem. Soc.* **2004**, *126*, 14708–14709.
(4) Cho, B. K.; Jain, A.; Gruner, S. M.; Wiesner, U. *Science* **2004**, *305*, 1598–1601.
(5) Sun, S. S. *Sol. Energy Mater.* **2003**, *79*, 257–264.
(6) Watkins, P. K.; Walker, A. B.; Verschoor, G. L. B. *Nano Lett.* **2005**, *5*, 1814–1818.
(7) Crossland, E. J. W.; Nedelcu, M.; Ducati, C.; Ludwigs, S.; Hillmyer, M. A.; Steiner, U.; Snaith, H. J. *Nano Lett.*, published online Oct 14, http://dx.doi.org/10.1021/nl800942c.
(8) Wang, H.; Oey, C. C.; Djurisic, A. B.; Xie, M. H.; Leung, Y. H.; Man, K. K. Y.; Chan, W. K.; Pandey, A.; Nunzi, J. M.; Chui, P. C. *Appl. Phys. Lett.* **2005**, *87*, 023507.
(9) Oey, C. C.; Djurisic, A. B.; Wang, H.; Man, K. K. Y.; Chan, W. K.; Xie, M. H.; Leung, Y. H.; Pandey, A.; Nunzi, J. M.; Chui, P. C. *Nanotechnology* **2006**, *17*, 706–713.
(10) Crossland, E. J. W.; Kamperman, M.; Nedelcu, M.; Ducati, C.; Wiesner, U.; Smilgies, D. M.; Toombes, G. E. S.; Hillmyer, M.; Ludwigs, S.; Steiner, U.; Snaith, H. *Nano Lett.*, published online Nov 14, http://dx.doi.org/10.1021/nl803174p.
(11) Andersson, S.; Hyde, S. T.; Larsson, K.; Lidin, S. *Chem. Rev.* **1988**, *88*, 221–242.
(12) Strom, P.; Anderson, D. M. *Langmuir* **1992**, *8*, 691–709.
(13) Schwarz, U. S.; Gompper, G. *J. Chem. Phys.* **2000**, *112*, 3792–3802.
(14) Hajduk, D. A.; Harper, P. E.; Gruner, S. M.; Honeker, C. C.; Kim, G.; Thomas, E. L.; Fetters, L. J. *Macromolecules* **1994**, *27*, 4063–4075.
(15) Schick, M. *Physica A (Amsterdam, Neth.)* **1998**, *251*, 1–11.
(16) Matsen, M. W.; Schick, M. *Phys. Rev. Lett.* **1994**, *72*, 2660–2663.
(17) Matsen, M. W.; Bates, F. S. *J. Chem. Phys.* **1997**, *106*, 2436–2448.
(18) Yu, B.; Li, B. H.; Sun, P. C.; Chen, T. H.; Jin, Q. H.; Ding, D. T.; Shi, A. C. *J. Chem. Phys.* **2005**, *123*, 234902.
(19) Rychkov, I. *Macromol. Theory Simul.* **2005**, *14*, 207–242.
(20) Martinez-Veracoechea, F. J.; Escobedo, F. A. *Macromolecules* **2005**, *38*, 8522–8531.
(21) Martinez-Veracoechea, F. J.; Escobedo, F. A. *J. Chem. Phys.* **2006**, *125*, 104907.
(22) Larson, R. G. *J. Phys. II* **1996**, *6*, 1441–1463.
(23) Gonzalez-Segredo, N.; Coveney, P. V. *Europhys. Lett.* **2004**, *65*, 795–801.
(24) Horsch, M. A.; Zhang, Z. L.; Glotzer, S. C. *J. Chem. Phys.* **2006**, *125*, 184903.
(25) Iacovella, C. R.; Keys, A. S.; Horsch, M. A.; Glotzer, S. C. *Phys. Rev. E* **2007**, *75*, 040801.

(26) Knorowski, C. D.; Anderson, J. A.; Travesset, A. *J. Chem. Phys.* **2008**, *128*, 164903.
(27) Ellison, L. J.; Michel, D. J.; Barmes, F.; Cleaver, D. J. *Phys. Rev. Lett.* **2006**, *97*, 237801.
(28) Dotera, T. *Phys. Rev. Lett.* **2002**, *89*, 205502.
(29) Matsen, M. W.; Bates, F. S. *Macromolecules* **1996**, *29*, 7641–7644.
(30) Hasegawa, H.; Hashimoto, T.; Hyde, S. T. *Polymer* **1996**, *37*, 3825–3833.
(31) Schroder-Turk, G. E.; Fogden, A.; Hyde, S. T. *Eur. Phys. J. B* **2007**, *59*, 115–126.
(32) Matsen, M. W. *Macromolecules* **1995**, *28*, 5765–5773.
(33) Matsen, M. W. *Phys. Rev. Lett.* **1995**, *74*, 4225–4228.
(34) Jain, A.; Toombes, G. E. S.; Hall, L. M.; Mahajan, S.; Garcia, C. B. W.; Probst, W.; Gruner, S. M.; Wiesner, U. *Angew. Chem., Int. Ed.* **2005**, *44*, 1226–1229.
(35) Martinez-Veracoechea, F. J.; Escobedo, F. A. *Macromolecules* **2007**, *40*, 7354–7365.
(36) Sknepnek, R.; Anderson, J. A.; Lamm, M. H.; Schmalian, J.; Travesset, A. *ACS Nano* **2008**, *2*, 1259–1265.
(37) Schultz, A. J.; Hall, C. K.; Genzer, J. *J. Chem. Phys.* **2002**, *117*, 10329–10338.
(38) Schultz, A. J.; Hall, C. K.; Genzer, J. *Macromolecules* **2005**, *38*, 3007–3016.
(39) Groot, R. D.; Warren, P. B. *J. Chem. Phys.* **1997**, *107*, 4423–4435.
(40) Groot, R. D.; Madden, T. J. *J. Chem. Phys.* **1998**, *108*, 8713–8724.
(41) Morse, D. C.; Tyler, C. A.; Ranjan, A.; Qin, J.; Thiagarajan, R. PSCF Home Page. http://www.cems.umn.edu/research/morse/code/pscf/home.php.
(42) Frenkel, D.; Smit, B. *Understanding Molecular Simulation: From Algorithms to Applications*, 2nd ed.; Academic Press: San Diego, CA, 2002.
(43) Lowe, C. P. *Europhys. Lett.* **1999**, *47*, 145–151.
(44) Lyubartsev, A. P.; Martsinovski, A. A.; Shevkunov, S. V.; Vorontsovvelyaminov, P. N. *J. Chem. Phys.* **1992**, *96*, 1776–1783.
(45) Escobedo, F. A.; Depablo, J. J. *J. Chem. Phys.* **1995**, *103*, 2703–2710.
(46) Bennett, C. H. *J. Comput. Phys.* **1976**, *22*, 245–268.
(47) Trebst, S.; Huse, D. A.; Troyer, M. *Phys. Rev. E* **2004**, *70*, 046701.
(48) Escobedo, F. A.; Martinez-Veracoechea, F. J. *J. Chem. Phys.* **2007**, *127*, 174103.
(49) Matsen, M. W. *J. Phys.: Condens. Matter* **2002**, *14*, R21−R47.
(50) Fredrickson, G. H.; Ganesan, V.; Drolet, F. *Macromolecules* **2002**, *35*, 16–39.
(51) Fredrickson, G. H. *The Equilibrium Theory of Inhomogeneous Polymers*; Oxford University Press: New York, 2006.
(52) Tyler, C. A.; Morse, D. C. *Macromolecules* **2003**, *36*, 3764–3774.
(53) Ranjan, A.; Qin, J.; Morse, D. C. *Macromolecules* **2008**, *41*, 942–954.
(54) Tyler, C. A.; Morse, D. C. *Macromolecules* **2003**, *36*, 8184–8188.
(55) Vassiliev, O. N.; Matsen, M. W. *J. Chem. Phys.* **2003**, *118*, 7700–7713.
(56) Matsen, M. W.; Griffiths, G. H.; Wickham, R. A.; Vassiliev, O. N. *J. Chem. Phys.* **2006**, *124*, 024904.
(57) Hajduk, D. A.; Harper, P. E.; Gruner, S. M.; Honeker, C. C.; Thomas, E. L.; Fetters, L. J. *Macromolecules* **1995**, *28*, 2570–2573.
(58) Matsen, M. W. *J. Chem. Phys.* **1998**, *108*, 785–796.
(59) Cochran, E. W.; Garcia-Cervera, C. J.; Fredrickson, G. H. *Macromolecules* **2006**, *39*, 2449–2451.
(60) Fredrickson, G. H.; Helfand, E. *J. Chem. Phys.* **1987**, *87*, 697–705.
(61) Abetz, V.; Simon, P. F. W. Phase Behaviour and Morphologies of Block Copolymers. In *Block Copolymers I*; Abetz, V., Ed.; Springer-Verlag: Berlin, Heidelberg, 2005; Vol. *189*, pp 125−212.
(62) Mareau, V. H.; Matsushita, T.; Nakamura, E.; Hasegawa, H. *Macromolecules* **2007**, *40*, 6916–6921.
(63) Martinez-Veracoechea, F.; Muller, E. A. *Mol. Simul.* **2005**, *31*, 33–43.

MA802427A